Electronic Supplementary Material (ESI) for Materials Horizons.

Supplementary materials for:

Bi-continuous Pattern Formation in Thin Films via Solid-State Interfacial Dealloying Studied by Multimodal Characterization

Chonghang Zhao[1], Kim Kisslinger[2], Xiaojing Huang[3], Ming Lu[2], Fernando Camino[2], Cheng-Hung Lin[1], Hanfei Yan[3], Evgeny Nazaretski[3], Yong Chu[3], Bruce Ravel[4], Mingzhao Liu[2], Yu-chen Karen Chen-Wiegart[1,3*]

[1] Department of Materials Science and Chemical Engineering, Stony Brook University, Stony Brook, NY 11794, U.S.A.

[2] Center for Functional Nanomaterials, Brookhaven National Laboratory, Upton, NY 11973, U.S.A.

[3] National Synchrotron Light Source II, Brookhaven National Laboratory, Upton, NY 11973, U.S.A

[4] Materials Measurement Laboratory, National Institute of Standards and Technology, Gaithersburg, MD 20899, U.S.A.

Email: Karen.Chen-Wiegart@stonybrook.edu

Supplementary video 1. A video based on the 3D XRF nano-tomography can be found in supporting information online.

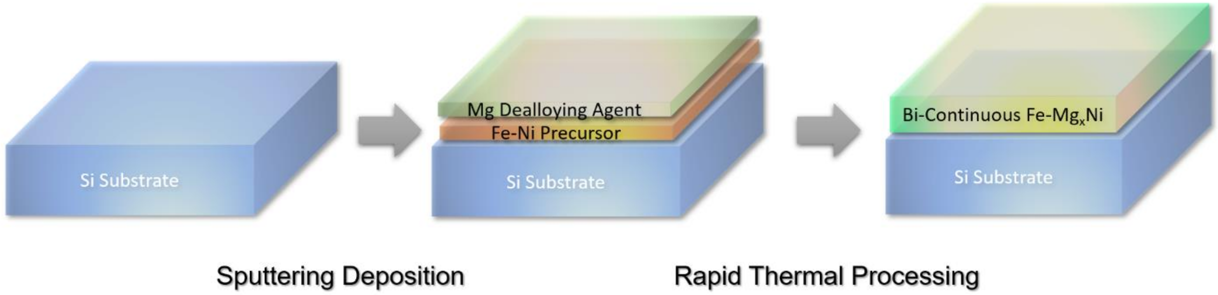

Figure S1. Schematic of solid-state interfacial dealloying process.

Primary and alternative hypotheses formulation and discussion on mechanisms:

The various completing or potentially co-existing mechanisms involved in the morphological evolution of this system should be carefully considered. The critical signature of dealloying, Fe-Ni+ Mg → Mg-Ni + Fe, that must be observed here would be 1) co-localization of Mg and Ni in elemental distribution, and segregation of Fe with Mg and Ni, as observed in STEM and XRF nano-tomography, and 2) chemically, Fe-Fe bonds would form, namely that Fe would have other Fe atoms as the coordination neighbors, as observed in XANES.

Here we also consider the alternative hypotheses:

A. If no reaction occurs, Fe-Ni + Mg remains, we should have observed: 1) Co-localization of Fe and Ni in elemental distribution, and segregation of Mg with Fe and Ni, 2) Chemically, Fe-Fe and Fe-Ni bonds co-exist, and an Fe atom would have some Ni atoms as its neighbors, and 3) no Mg-Ni compound formation.
B. If phase separation of Fe-Ni occurs, which was not introduced by Mg dealloying, Fe-Ni → Fe + FeNi3, we should have observed: 1) Co-localization of Fe and Ni, as well as some segregation of Fe, Ni and Mg. No co-localization of Mg and Ni would be observed.
C. If the system forms a solid solution, Fe-Ni + M → Fe-Ni-Mg, we should have observed the co-localization of Fe, Ni and Mg.

We summarized the above consideration in a table below:

Hypothesis	Pathway	Elemental distribution	Fe environment (Chemical and Structural)
Dealloying of Fe-Ni by Mg	Fe-Ni + Mg → Mg-Ni + Fe	Mg and Ni co-localization Fe individual phase	Mainly Fe-Fe coordination
Alternative A. No reaction	Fe-Ni + Mg	Fe and Ni co-localization Mg individual phase	Fe-Fe and Fe-Ni coordination
Alternative B. Phase separation of Fe-Ni	Fe-Ni + Mg → Fe + FeNi3 + Mg	Fe and Ni co-localization Fe, Mg individual phases	Fe-Fe and Fe-Ni coordination
Alternative C. Form a solid solution	Fe-Ni + Mg → Fe-Ni-Mg	Fe, Ni, Mg co-localization	Fe-Fe, Fe-Ni and Fe-Mg coordination

The elemental distribution was studied by STEM (Fig. 1) and XRF nano-tomography (Fig. 2), the Fe environmental was studied by XANES (Fig. 4d), with TEM diffraction also identifies potential compounds in the system (Fig. 4a-c), especially Ni-Mg compounds. Our experimental results support the hypothesis of dealloying of Fe-Ni by Mg.

Below we consider the details in isothermal treatment and the corresponding potential phases during the heat treatment, as well as during the cooling stage; this is to ensure that the observation is consistent with the prediction of thermodynamics. First, during the heat treatment, the samples were heated to 460 ^{o}C, and in this dealloying process, we heat and cool the samples. At this elevated temperature, according to the phase diagram, we do not expect the phase separation of γ – (Fe, Ni) into Fe and $FeNi_3$. Thus, due to the presence of Mg phase, the dealloying is expected to occur at this elevated temperature, leading to the formation of Fe and Mg-Ni phases. During cooling, these two phases are stable and should be present at the room temperature. Thus we think that the dealloying of Fe-Ni by Mg is the most likely pathway, and thus our primary hypothesis; this work tested this hypothesis and provided the evidence to support this hypothesis.

Type	Condition	Sample ID	Analysis
Thin	Pristine Fe-Ni / Mg	S100-P1	TEM/SAED, SEM/EDX
		S100-P2	XANES
	460°C 30min Fe-Ni / Mg	S100-D1	STEM/EDX, TEM/SAED
		S100-D2	XRF nano-tomography/Ptychography
		S100-D3	XANES
		S100-D4	SEM/EDX top
	460°C 30min Ni / Mg	S100-K	SEM (for Kirkendall effect study)
Thick	Pristine	S300-P	SEM/EDX
	460°C 30min	S300-D	SEM/EDX
	430°C 7.5min	S300-D-L	SEM/EDX

Table S1. List of samples with different treat conditions and methods of characterization. For sample ID notation – S: sample, P: pristine, D: dealloying, K: Kirkendall effect, L-S: lower temperature/short time

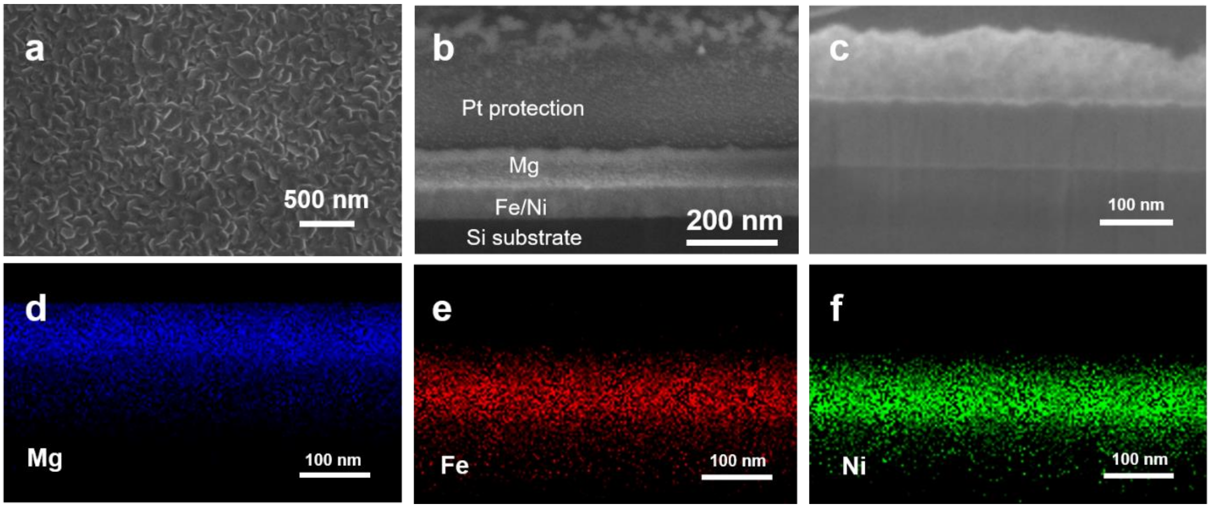

Figure S2. The SEM images of pristine, Fe-Ni and Mg thin films as deposited on the Si substrate (S100-P1): **a** The top view and **b** the cross-section view; from the top to bottom the images shows the Pt protection layer for FIB fabrication, Mg layer, Fe-Ni film and Si substrate. The high magnification SEM cross-section view with EDX analysis are shown in **c-f**.

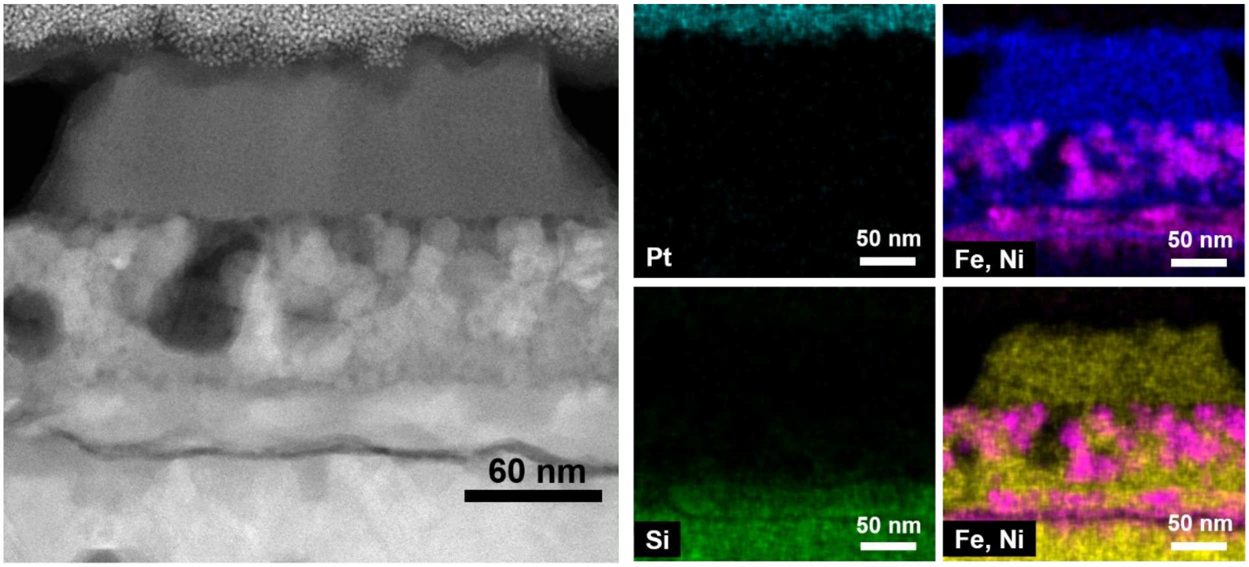

Figure S3. STEM analysis of, Fe-Ni dealloyed with Mg at 460°C for 30 min (S100-D1), other elements in the system are included.

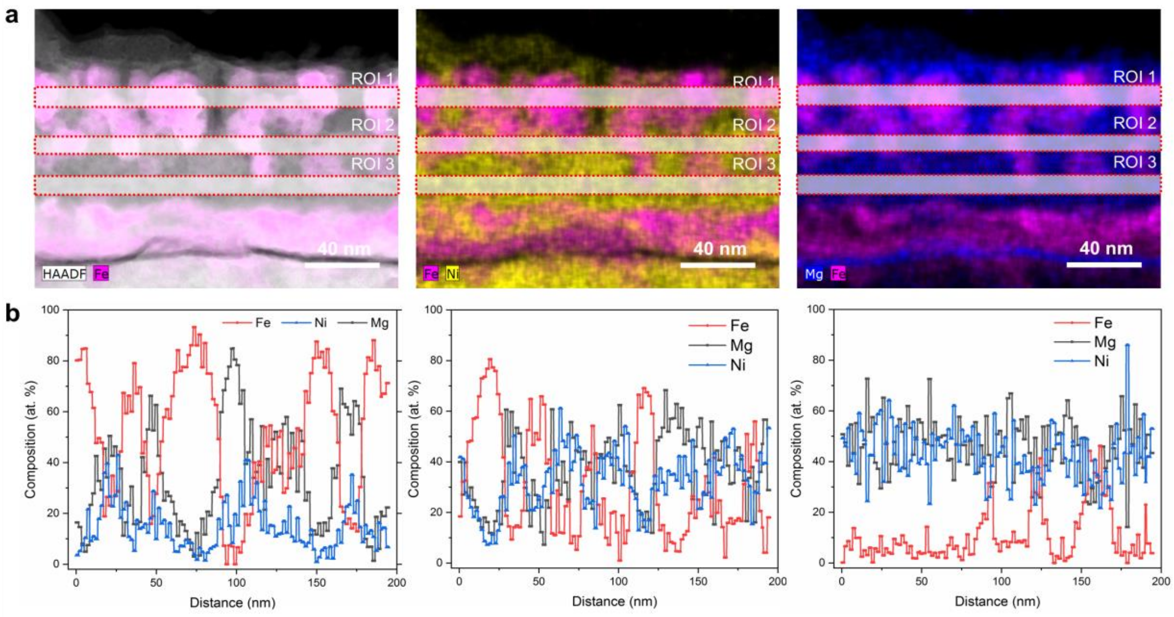

Figure S4. (a) Overlap of HAADF with Fe EDX mapping, Fe and Ni EDX mapping, and Fe with Mg EDX mapping. The selected ROIs are shown in the figure. (b) Composition collected by line scan through EDX mapping. From the left to right are collected from ROI1, ROI2 and ROI3.

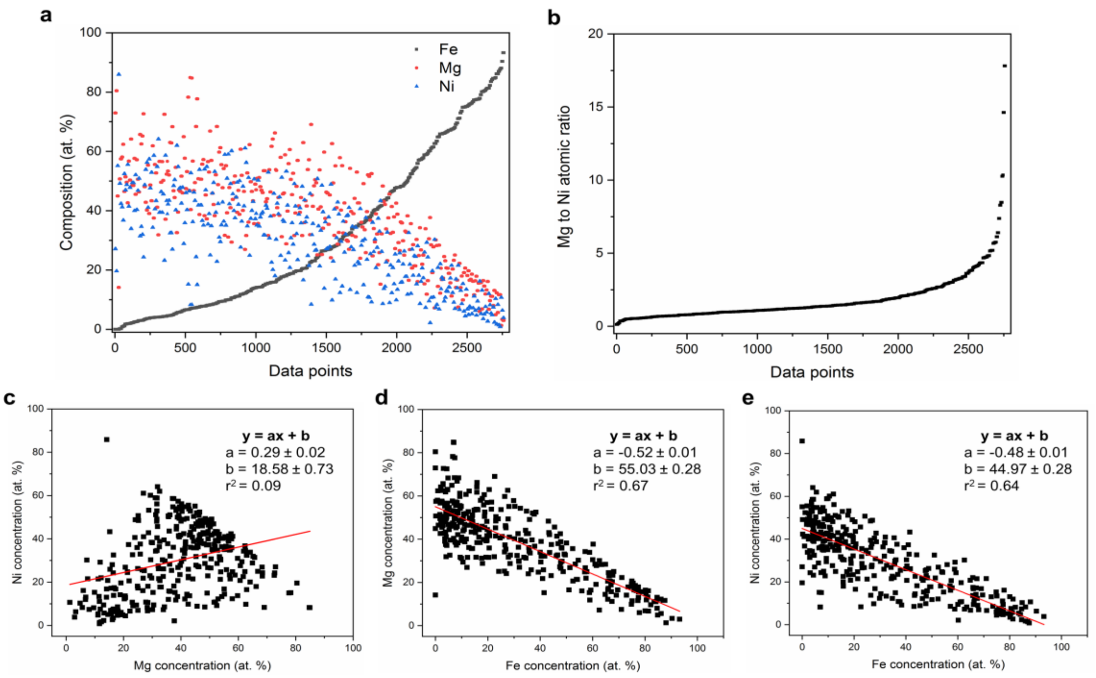

Figure S5. (a) Plotting of Mg, Ni and Fe atomic concentration collected from three ROIs. Note that data points were sorted from low-to-high Fe concentration. (b) Atomic ratio between Mg and Ni plotted from three ROIs. (c-e) Atomic concentration correlation with linear fitting between Mg-Ni, Fe-Mg and Fe-Ni.

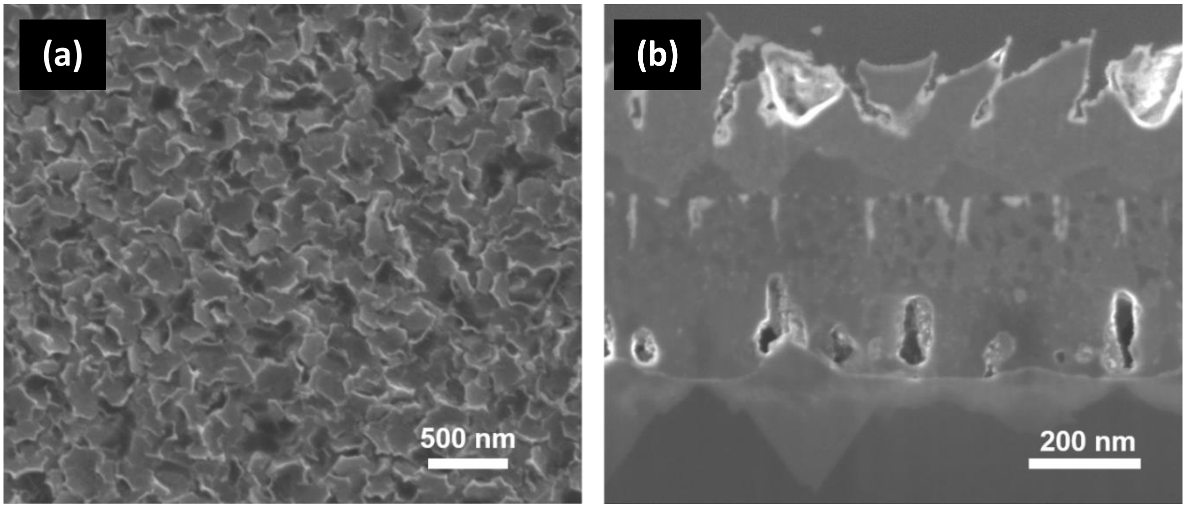

Figure S6. SEM images of a thicker sample (S300-D), Fe-Ni film dealloyed at 460˚C for 30 min. (a) The top view and (b) the cross-section view.

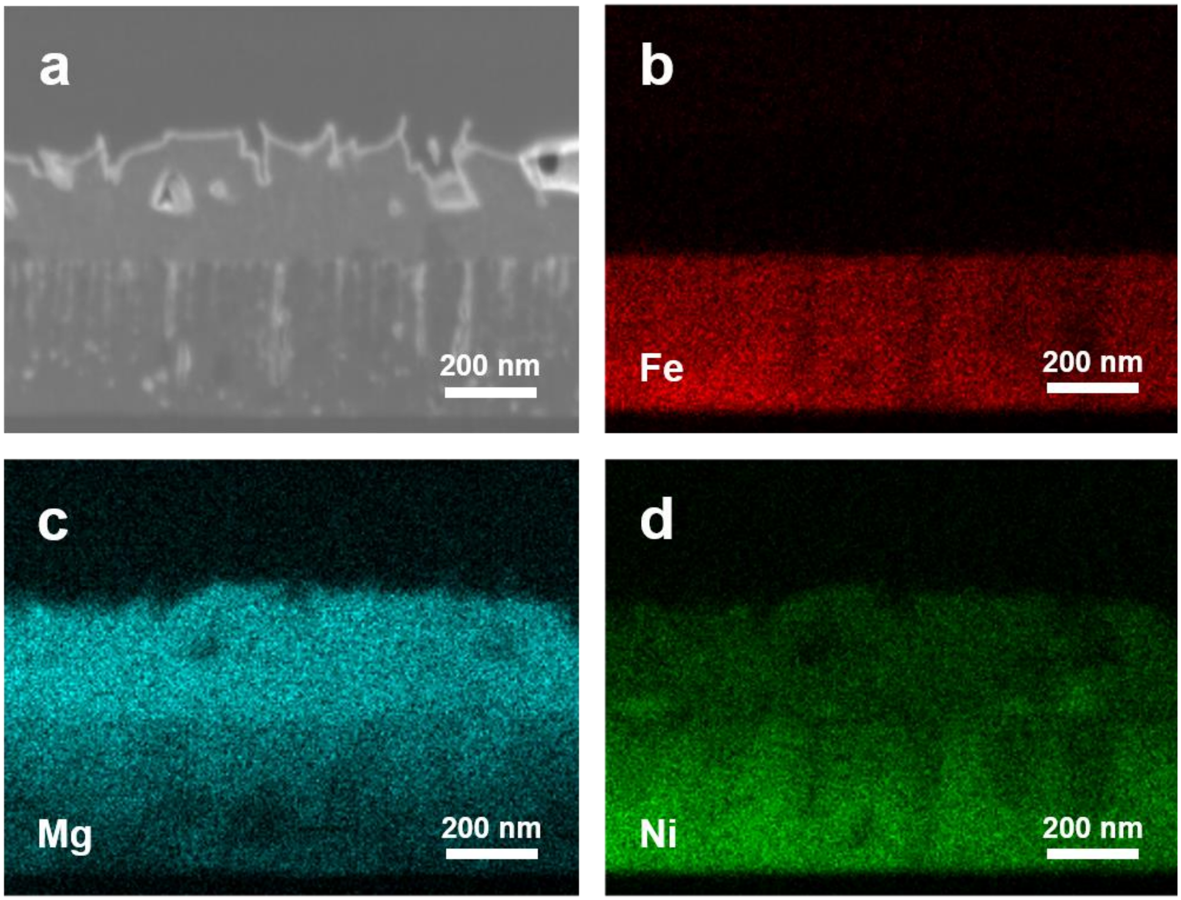

Figure S7. SEM and EDX analysis from cross-section view of a thicker sample (S300-D-L), Fe-Ni film dealloyed at 430˚C for 7.5 min. (a) SEM of the cross-section showing the EDX analysis area. EDX analysis showing elemental distributions: (b) Fe, (c) Mg and (d) Ni.

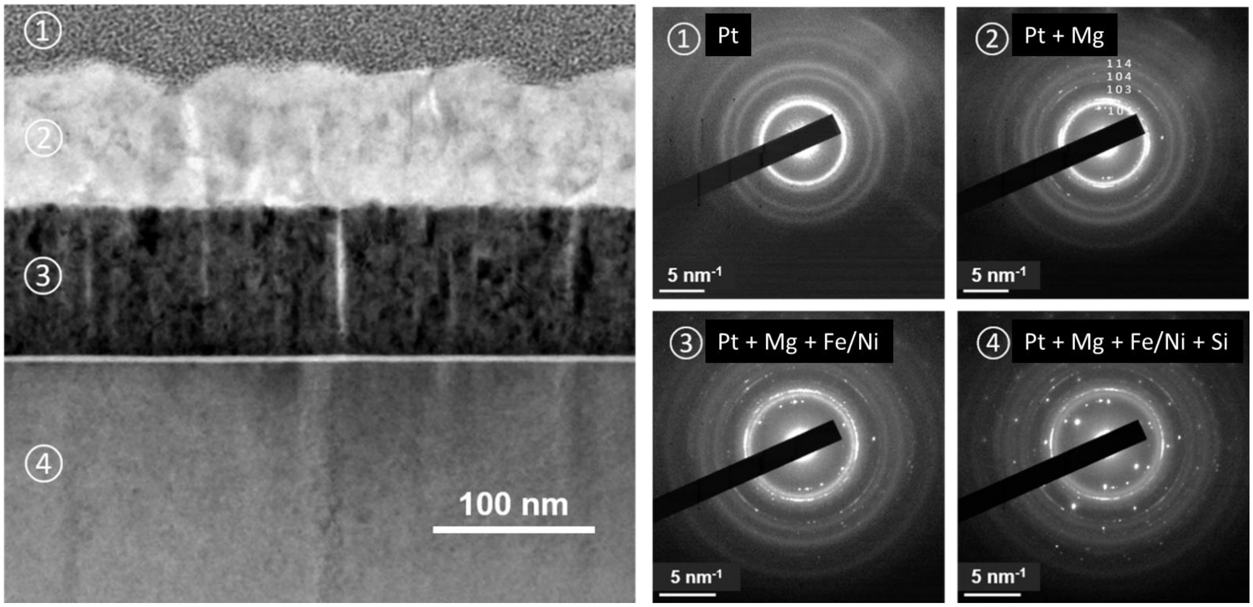

Figure S8. TEM image and electron diffraction from each layer of as-deposited sample (S100-P1), Mg, Fe-Ni thin films on the silicon substrate. Due to the limited SAED aperture size, the SAED pattern does not correspond to the individual layer's film thickness. The TEM image and SAEDs were collected by moving the sample gradually into the field of view of SAED, from the top to the bottom layers of the sample, and the results include (1) Pt protection layer, (2) Pt with Mg as deposited layer, (3) Pt with Mg and Fe-Ni as deposited layer, and (3) whole films with Si substrate.

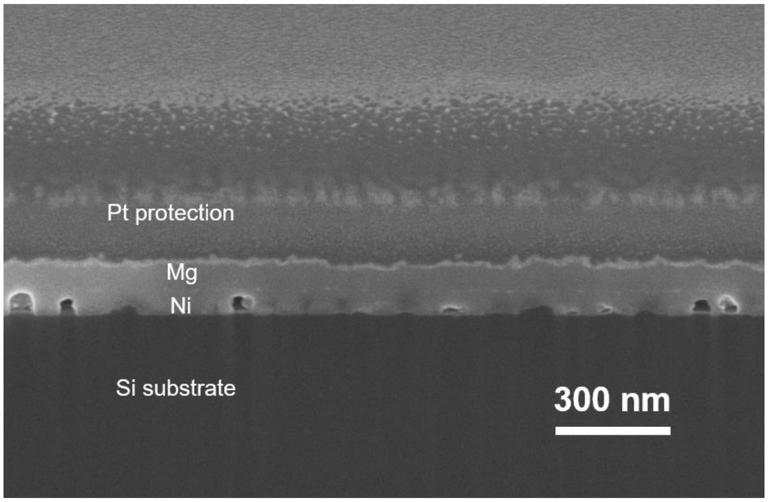

Figure S9. Cross-section of the controlled sample (S100-K), with Ni and Mg sequentially deposit onto the Si substrate. On the top is the Pt protection layer.

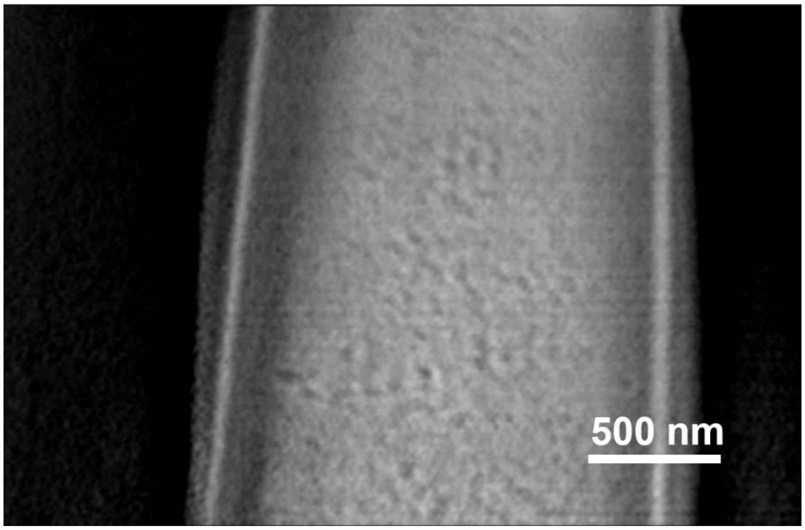

Figure S10. Reconstructed ptychography result from sample S100-D2, collected from the direction that film perpendicular to the incident beam.

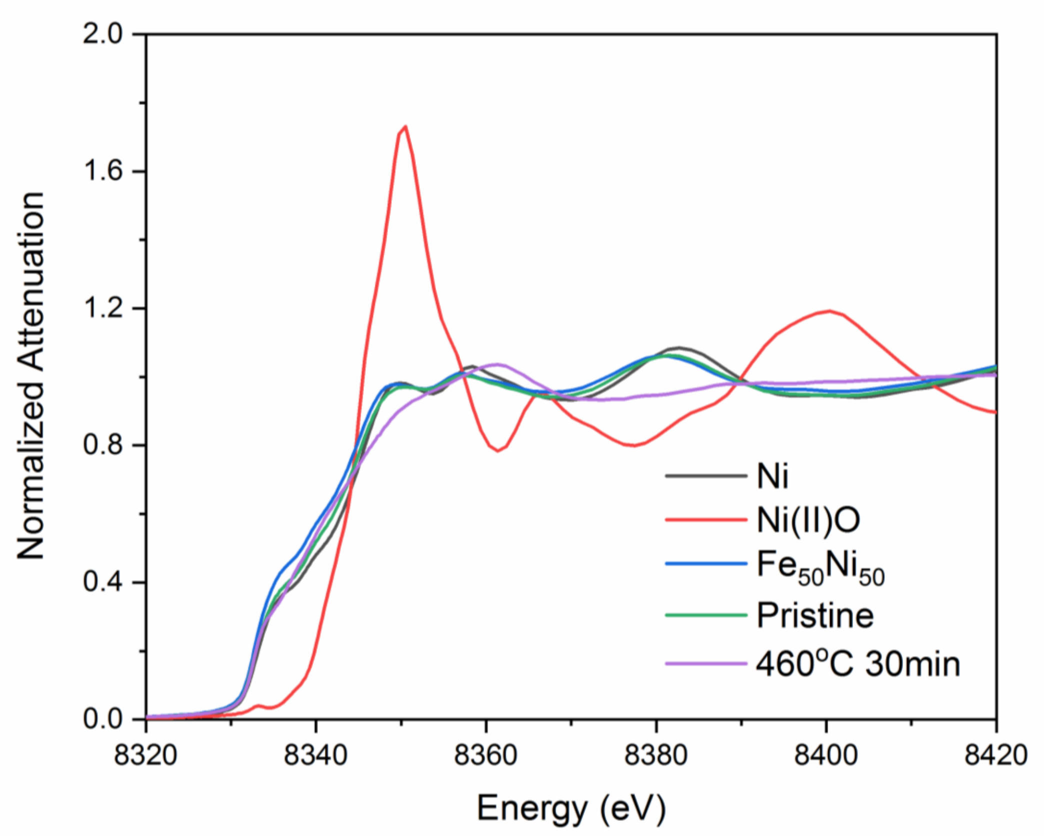

Figure S11. XANES at the Ni edge of Ni foil standard, Ni(II)O powder standard, Fe-Ni (50-50 at.%) powder standard, Pristine sample (S100-P2) and sample after dealloyed at 460˚C for 30min (S100-D3).

Quantification of pristine films

We conducted careful analysis on the pristine samples used in this study. Although we used Fe-Ni 50-50 at% target in our sputtering process, it is known from the literature and from the experiences of working with sputtering that the deposited film composition could differ from the target composition, with the extent differs from system to system. This can be attribute to different sputtering yield from different elements.

We used EDX in SEM, a semi-quantitative method, to study the composition of deposited film and found that the deposited film composition is close to Fe-Ni 25-75 at%, with Fe 25.86 at. % and Ni 74.14 at. %, standard division of 1.218 at. %. This value, despite instrumentation calibration conducted by the instrumentation staff, may still be an over-estimation of Ni due to the less self-absorption of Ni fluorescence signal through the films. While the film thickness is thin, and the self-absorption effect should be negligible, depending on the geometry of the detector-sample and the solid-angle of the detector, the effective thickness may be high. In addition, we quantified the XRF mapping results from the X-ray nano-probe analysis from the HXN beamline; assuming no mass loss during dealloying and the sample within the scanned region is representative of all regions, the analysis result from dealloyed film indicates a composition of Fe-Ni as 36.31-63.69 at. %, with standard division of 0.267 at. %. This is taken by averaging all frames of the tomographic data collected, and thus better reflect the actual compositions; while a slight over estimation of the Ni composition may still be persist here due to the same self-absorption effect mentioned above. STEM analysis could also be conducted from the dealloyed sample but due to the limited scanned area in STEM, we believe that the HXN data conducted from the same sample better reflects the overall sample composition in this case.

One possible method in future study to better control the pristine film composition is co-sputtering two materials together and tuning the deposition parameters to reach designed composition. Calibration experiment with known standard may be conducted to understand the instrumentation limitation in quantifying the relative ratio between Ni and Fe in EDS and nano-probe XRF. ICP-type of quantification may also be conducted. Including further XRF self-absorption may be done however only with detailed calculation involved the detector-to-sample geometry and knowledge of the sample structure itself, e.g. with an iterative calculation of such, which can be included in future work.